Pergamon

Atmospheric Environment Vol. 29, No. 16, pp. 2139–2155, 1995

1352–2310/95 $9.50 + 0.00

1352-2310(94)00141-3

SENSITIVITY OF MONSOON CIRCULATIONS TO CHANGES IN SEA SURFACE TEMPERATURES

KIRAN ALAPATY, SETHU RAMAN,† U. C. MOHANTY* and R. V. MADALA†

Department of Marine, Earth and Atmospheric Sciences, North Carolina State University, N.C. 27695-8208, U.S.A.; *Centre for Atmospheric Sciences, Indian Institute of Technology, New Delhi-110 016, India; †Naval Research Laboratory, Washington, D.C., 20375, U.S.A

(*First received* 20 *March* 1993 *and in final form* 22 *December* 1993)

Abstract—Sensitivity of a regional scale model to different sea surface temperatures (SSTs) in the context of short-range prediction of monsoon rainfall is studied using a three dimensional regional scale model. For the month of July, over certain regions of Arabian Sea, Bay of Bengal and the Indian Ocean, observed SSTs are about 1 to 2°C warmer than the climatological SSTs. Two numerical experiments are performed using observed and climatological SSTs for an active monsoon period. It is found that the evaporation increases over these surrounding oceans when the observed SSTs are used. As expected, warmer SSTs caused the surface pressure to decrease by 2 to 3 hPa leading to local accelerations of winds. As a result, stronger circulation patterns are induced. Area-averaged evaporation is about 20% higher and the rainfall 10% higher when observed SSTs are used.

Effect of an uniform increase in SST by 2°C over climatological values is also investigated. Comparison of simulations with the climatic and the uniformly increased SSTs indicated that the rainfall predictions are qualitatively similar to those obtained with the observed SSTs. Area-averaged evaporation is about 40% higher and the rainfall 15% higher than those obtained with the climatic SSTs.

Results from these three numerical experiments indicate that the short-range prediction of monsoon weather is sensitive to the sea surface temperature distribution. This is mainly because of variations in mesoscale circulations caused by the local gradients in the SSTs.

Key word index: Monsoon, Sea surface temperature, Rainfall, Anomalies.

1. INTRODUCTION

The Indian southwest monsoon is characterized by strong northward cross-equatorial flow of moist air off the east coast of Africa as indicated in several studies (e.g. Saha and Bavadekar, 1973; Cadet and Reverdin, 1981) along with a low-level jet over the Arabian Sea. Two dominant features of the monsoon region are (1) change in the direction of the prevailing winds by at least 120° between winter and summer seasons, and (2) spells of heavy rainfall during the monsoon period. Based on these criteria, the region between 25° S to 35° N and 30° E to 170° E can be considered as the monsoon region (Ramage, 1971). Monsoon westerlies in the lower troposphere approach the west coast of India almost at right angles to the Western Ghat mountain ranges after traveling thousands of kilometers over the warm Indian Ocean and the Arabian Sea. Prevailing local convective instability triggers deep convection giving rise to large rainfall over the Indian subcontinent. Low pressure depressions often develop over Bay of Bengal during the active periods of monsoon. These depressions some times develop into intense tropical cyclones, giving rise to large rainfall over northeastern sectors of India. A low level jet called Somali jet over the Arabian Sea whose roots originate in the Mozambique Channel (Van de Boogard and Rao, 1984) is also associated with summer monsoon flow. The core of the Somali jet is situated at an altitude between 1 and 2 km and its separation from African coast appears to occur around 10° N.

Ocean–atmosphere interactions over the Arabian Sea play an important role affecting the dynamics and the thermodynamics of the monsoon region. A numerical modeling study by Shukla (1975) using a general circulation model indicated that cold SST anomaly over a western part of the Arabian Sea would decrease the rainfall over India. In contrast, a similar study by Washington *et al.* (1977) suggested that SST anomalies over the Arabian Sea may not have substantial effect on the rainfall over the Indian subcontinent. Some observational studies (Anjaneyulu, 1980; Jospeh and Pillai, 1984; Kusuma and Goswami, 1988) show positive correlation between monsoon rainfall and premonsoon SST anomaly while other observational studies (Weare, 1978; Ramesh Babu *et al.*, 1989) indicate either no correlation or even negative correlation.

These studies were made in the context of long-range (seasonal) forecast of monsoon rainfall over the Indian subcontinent linking the SST anomalies over the Arabian Sea. The contradicting results obtained from these climate models depend highly on the model physics rather than the initial conditions, and hence subject to uncertainties in the physics used. Also, the above mentioned observational studies used observed SST data over relatively smaller regions of the Arabian Sea. Observational data covering most of the Arabian Sea are required for evaluating the effects of warm and cold anomalies on the monsoon rainfall. Thus, the effects of SST variation on short-range monsoon rainfall forecast has not yet been studied. The objective of this paper is to study the sensitivity of the monsoon rainfall to the observed daily SSTs and climatological SSTs using a three dimensional regional scale model. For this purpose we have chosen to simulate the monsoon rainfall for the days 17 and 18 July 1988 during which large rainfall rates were observed.

2. THE MODEL

The Naval Research Laboratory and North Carolina State University (NRL/NCSU) regional scale model is used in the present study. It is a primitive equation model written in pressure-based σ-coordinate system having a one-way interacting nested grid network. The σ-coordinate is defined by $\sigma = p/p_s$, where p is the pressure and p_s the surface pressure. For further model details, readers are referred to Madala *et al.* (1987). Various physical processes are included in the model either explicitly or in parameterized form and these are discussed below.

2.1. *Physical processes*

The model physics includes latent heat, sensible heat, and momentum exchange between the boundary layer and the underlying surface using the surface layer similarity theory (Businger *et al.*, 1971), grid-scale precipitation, dry convection, and diffusion processes. The short-and long-wave radiative processes are not included in the present model. A second-order diffusion for momentum on σ-surfaces and for heat and water vapor on p-surfaces is used to account for the cascading of energy into unresolved subgrid-scale waves. If supersaturation exists at any level, the excess moisture is assumed to condense and fall out to the next lower layer and evaporate or continue to fall depending upon the degree of the saturation at that level. The model has a dry convective adjustment procedure to remove dry convective instability that can occur during model integration. The cumulus convection parameterization scheme developed by Kuo (1965, 1974) is used in the model simulations. The moistening parameter b is calculated according to the method suggested by Anthes (1977) and is given by

$$b = [1 - \langle \mathrm{RH_g} \rangle]^n, \tag{1}$$

where $\langle \mathrm{RH_g} \rangle$ is the mean environmental relative humidity. We have used $n = 3$ for the moisture partitioning in the equation (1) consistent with the study on the convective heating rates over the monsoon region (Das *et al.*, 1988).

2.2. *Numerical methods*

The time integration scheme utilized in the present model is a split-explicit method which allows a larger time step by effectively separating various terms in the prognostic equations into parts governing slow-moving Rossby modes and fast-moving gravity modes. For the first and second fast-moving gravity modes smaller time step is used and for all other modes a larger time step is used. The implementation of these varying time steps is the basis for the split-explicit method. The time steps for the slow moving modes in the coarse-grid and the fine-grid domains are 300 and 100 s, respectively, and appropriate smaller time steps satisfying CFL criterion are used for the fast-moving modes. For the horizontal differencing, a staggered grid network (Arakawa C-grid) is used with p_s, q, T, ϕ, σ specified at the same horizontal points, and u and v interlaced between them where p_s is the surface pressure, q the specific humidity, T the temperature, ϕ the geopotential, $\dot{\sigma}$ the vertical velocity of σ, u the zonal wind velocity, and v the meridional wind velocity, respectively. The finite difference technique used in the model is second-order accurate. It conserves total energy, mass, and momentum in the absence of the heat and momentum sources.

2.3. *Data and simulation domain*

Simulation domain is shown in the Fig. 1 and the domain covers from 37.5° E to 112.5° E and 20.5° S to 42.5° N. Model topography was obtained from the navy 10′ global topography data. Initial conditions are obtained from the European Center for Medium-Range Weather Forecasts (ECMWF) analysis. Horizontal resolution of the anlyzed data obtained from the ECMWF is 1.875° × 1.875°, available at 14 vertical levels. Horizontal grid resolution in the model is 1.5° and the vertical grid resolution in σ-coordinate is 0.1. The lateral boundary conditions are obtained from the ECMWF analysis and are merged with the forecast values using the scheme of Davies (1976, 1983). At the model top and bottom, the boundary condition used for $\dot{\sigma}$ is zero.

2.4. *Numerical experiments*

To achieve the objective of this study, two numerical simulations are performed for 48 h starting at 12 UTC 16 July 1988. Model sea surface temperatures in the first numerical experiment are obtained through interpolation from 1° resolution global climatological values based on a 10 year average for the month of July. In the second numerical experiment model sea surface temperatures are obtained from the average of daily analyzed SSTs for the period 16 July to 18 July, 1988. Daily SST data are analyzed by the ECMWF utilizing the satellite and ships data and are available at 1.875° × 1.875° resolution. Results from the experiment using the climatological SSTs and observed SSTs are referred to as SSTC and SSTO, respectively.

2.5. *Synoptic conditions*

Monsoon trough is one of the low-level features associated with the monsoon circulations. The orientation and its geographical location changes with the advancement of the monsoon. During the active monsoon period the monsoon trough has a northwest orientation with the northern tip located near the foothills of the Himalayas and the southern tip over the Bay of Bengal. Often low-pressure centers develop when the monsoon trough structure is observed as described above. These low-pressure centers develop into monsoon depressions and some times into tropical cyclones giving rise to large rainfall rates over India. When the monsoon was active large rainfall rates, due to the orographic lifting and associated convection, are observed over the west coast of India. Also, presence of a monsoon depression over the Bay of Bengal causes stronger circulation patterns along the west coast of India leading to larger rainfall rates over this region.

Monsoon was active during the simulation period (12 UTC 16 July to 12 UTC 18 July) and large rainfall rates were observed. A monsoon depression was present over the Bay of Bengal close to the east coast of India. Analyzed streamline

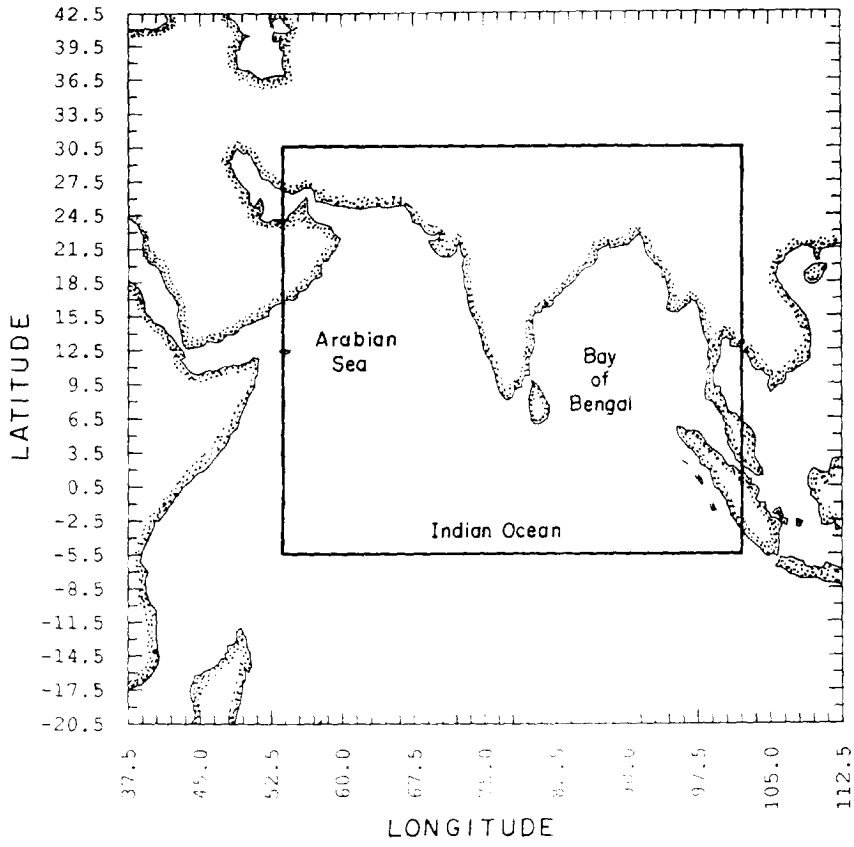

Fig. 1. The model domain of numerical simulation.

distribution and horizontal winds for the 850 hPa at 12 UTC 16 July 1988 (initial conditions) are shown in Fig. 2. Cyclonic circulations over the Bay of Bengal close to the east coast of India indicate the location of the monsoon depression. This depression has moved northwest and made landfall during the next 24 h and moved further inland and was located over northeast India at 12 UTC 18 July. Large rainfall rates were reported over northeast India resulting from the monsoon depression. Strong winds (broken lines are isotachs) off the east coast of Africa are due to the presence of Somali jet over this region. The interaction of Somali jet with the monsoon circulation and its impact on the monsoon dynamics is still not well understood. Analyzed mean sea level pressure distribution at 12 UTC 16 July 1988 is shown in Fig. 3. The low-pressure center (monsoon depression) is consistent with the location of the cyclonic circulations seen in Fig. 2. Low-pressure center over west India is due to the strong heating over the desert regions and is called the heat-low.

3. DISCUSSION OF RESULTS

In this section, results from the SSTC and the SSTO are analyzed to find the differences between the forecasts. Coast lines were determined based on the topography data. Thick solid lines in all figures represent the coast lines.

3.1. *Sensitivity to the sea surface temperatures*

Climatological sea surface temperature distribution for the month of July is shown in Fig. 4a and the differences between the three-day averaged observed and climatological SSTs are shown in the Fig. 4b. As can be seen from Fig. 4b that over the open oceans observed SSTs are about 1 to 2°C warmer than climatological values while some stronger gradients exist along the coastal areas. Also, it can be seen that differences in the SSTs are not confined to a particular region over the oceans. Differences between the surface pressures predicted by the SSTO and the SSTC at the end of 48 h (12 UTC 18 July) of simulation are shown in Fig. 5a. As expected, presence of positive SST anomalies led to mesoscale regions of lower surface pressures. Increased convergence over oceanic regions caused stronger circulation patterns thereby affecting the circulations over adjoining land regions. Differences between horizontal wind speeds at the model's lowest level predicted by the SSTO and the SSTC at the end of 48 h are shown in Fig. 5b. Spatial distribution of these differences in the wind speeds are consistent with the spatial distribution of the differences between the surface pressures in the SSTO and the SSTC. Similar results were also found in a numerical study (Shukla, 1975) using a global model when anomalies were introduced into the climatological SSTs.

The presence of warm anomaly in the sea surface temperature and the increase in low-level wind

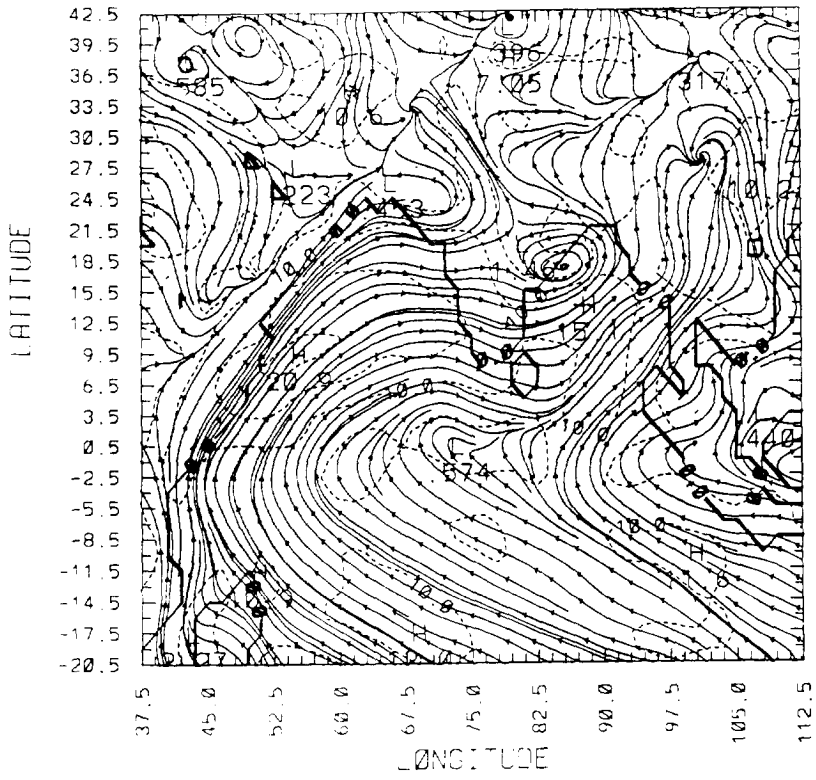

Fig. 2. Analyzed horizontal streamline and wind distribution at $\sigma = 0.85$ at 12 UTC 16 July 1988 (initial conditions). Contour interval is 5 m s^{-1}.

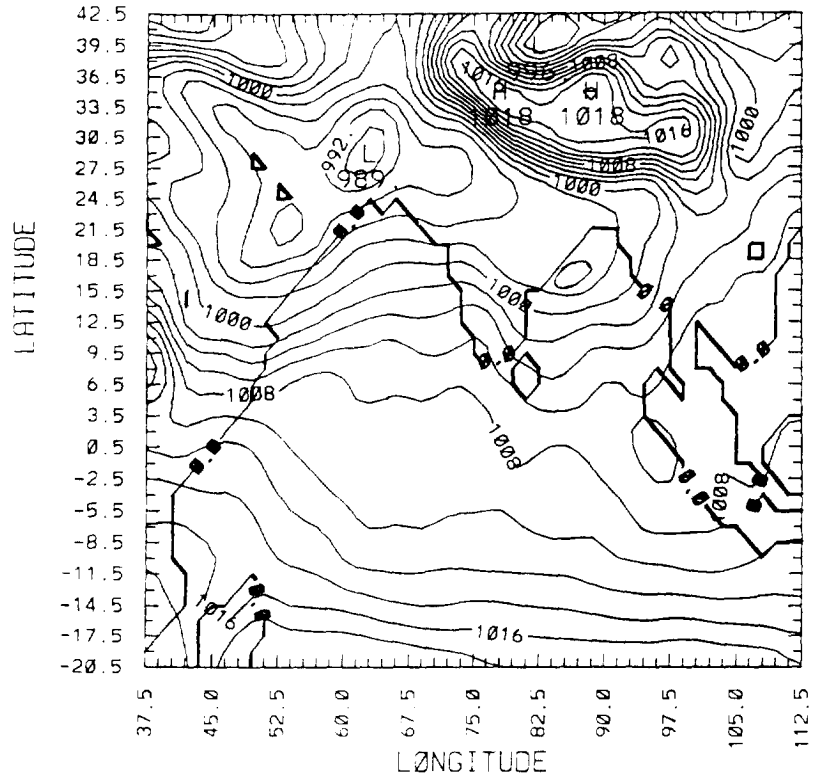

Fig. 3. Analyzed mean sea level pressure at 12 UTC 16 July 1988 (initial conditions). Contour interval is 2 hPa.

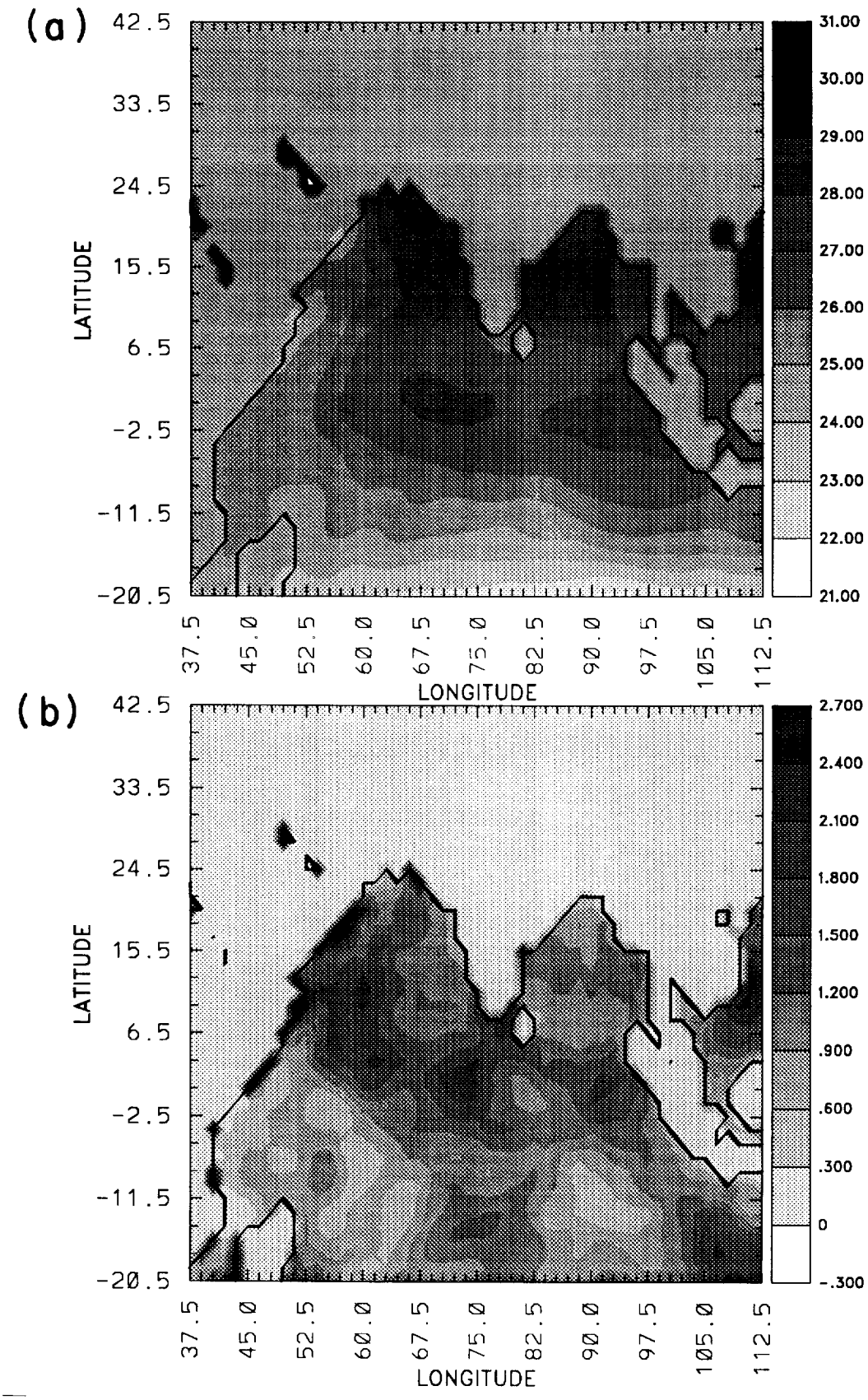

Fig. 4. (a) Climatological sea surface temperature distribution (C) for the month of July and (b) the differences between the three-day averaged and climatological SSTs.

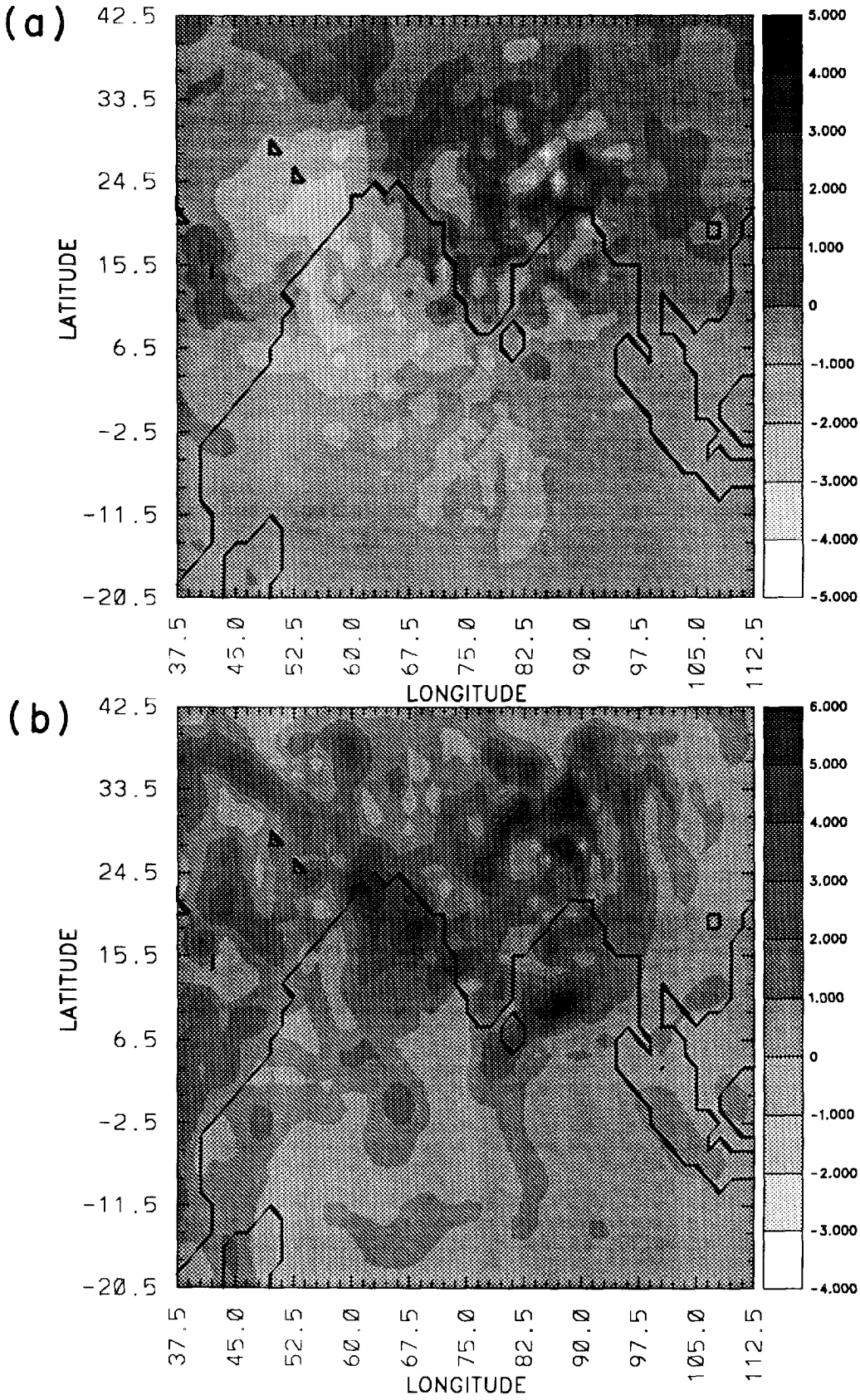

Fig. 5. Differences between the simulations in the SSTO and SSTC at the end of 48 h for (a) the surface pressures (hPa) and (b) the surface horizontal winds ($m\,s^{-1}$).

speeds should lead to increase in evaporation. Differences between the daily averaged latent heat fluxes predicted by the SSTO and SSTC at the end of 48 h of simulation are shown in Fig. 6. The results indicate that evaporation is increased by about 100 to 200 W m^{-2} locally. These differences are higher over the location of the Somali jet (east coast of Africa), northern Arabian Sea and southern Bay of Bengal. Enhanced mesoscale convergence caused by local SST gradients and increased evaporation should lead to larger rainfall.

Large rainfall rates were observed over the west coast of India (Fig. 7a) and were due to orographic-convective processes. For the two days of simulation, observed rainfall rates were about 100–200 mm d^{-1} along the west coast of India. The rain gage data analysis by Ramakrishnan and Gopinatha Rao (1958) and Ramachandran (1972) revealed that the intense rainfall is concentrated upstream (seaward) of the Western Ghats. Offshore extension of this rainfall for the 1979 monsoon was documented by Krishnamurti *et al.* (1983) using a combined analysis of satellite and rain gage data. Rainfall rates of about 70 mm d^{-1} (Fig. 7a) over the central regions and east coast of India were due to presence of a monsoon depression. During the next 24 h, monsoon depression moved northwest and has weakened. This resulted in decreased rainfall rates over this region (Fig. 7b).

Predicted rainfall distribution by the SSTC for a period of 24 h ending at 12 UTC 17 July is shown in Fig. 7c. Analyzed data indicated presence of strong winds southwest of the monsoon depression and is a general feature associated with the monsoon depressions (Rao, 1976). Model also predicted rainfall over the southwest section of the monsoon depression. Spatial distribution of the rainfall over central India is also consistent with the observed rainfall. Rainfall associated with the orography along the west coast of India is well predicted with maximum located just offshore which is consistent with the generally observed pattern. Model-predicted rainfall distribution by the SSTC for a period of 24 h ending at 12 UTC 18 July is shown in Fig. 7d. Predicted rainfall along the monsoon trough region is smaller than those predicted during the first day of simulation. Along the west coast of India spatial distribution of rainfall is some-

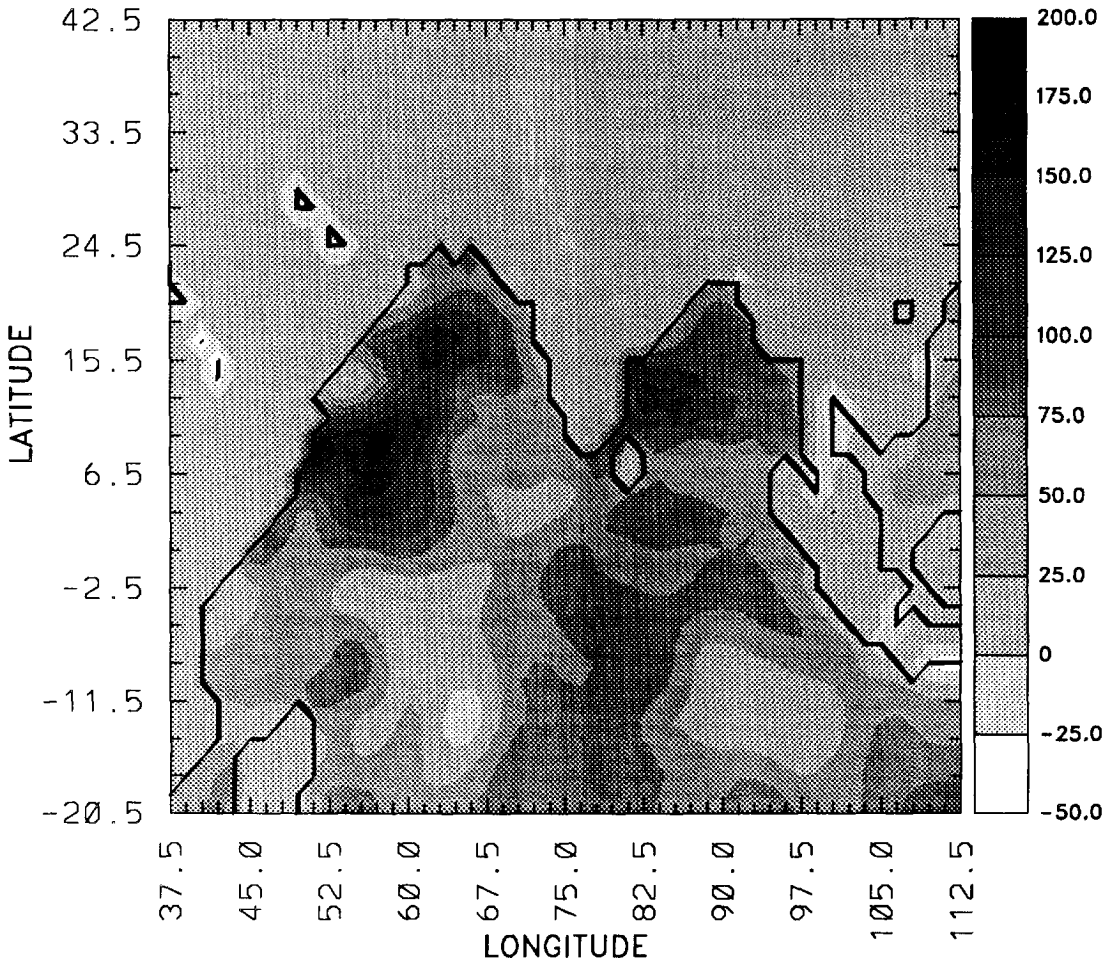

Fig. 6. Differences between the predicted mean latent heat fluxes (W m^{-2}) in the SSTO and the SSTC at the end of 48 h.

were similar to that during the previous day. In general, predicted rainfall is larger over the depression region during the first day of simulation than that during the second day, consistent with the observations. However, over the Western Ghats region predicted rainfall rates are somewhat lower when compared to observations. This is due to coarse resolution and bulk boundary layer physics used in the model. Predicted rainfall over the lake (15° N, 37° E) is not readily verifiable due to lack of observations. However, predicted rainfall over Somalia (desert regions) during the first day of simulation is not consistent with the observations. This is due to the presence of errors in the initial conditions. Since analyzed fields are

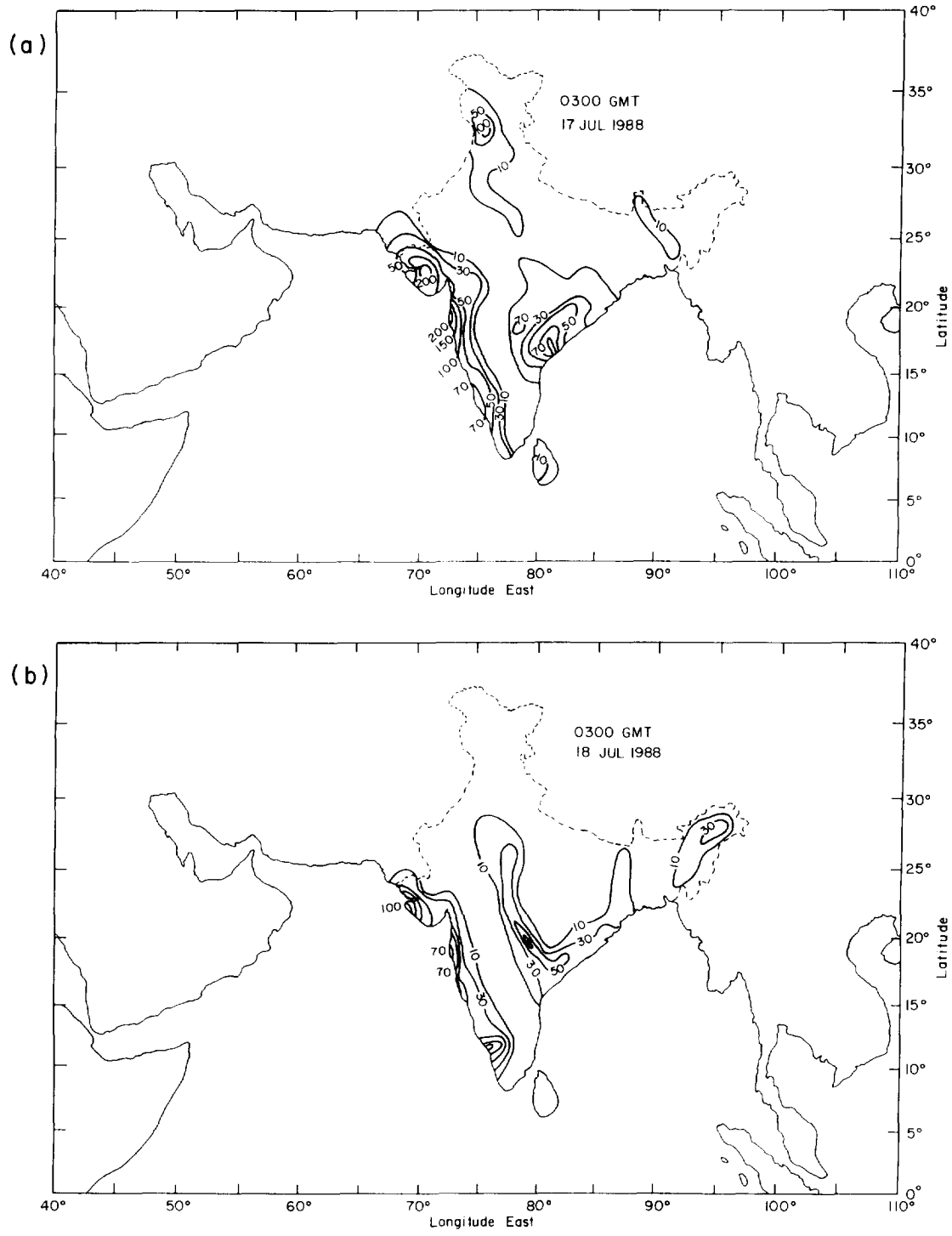

Fig. 7a, b.

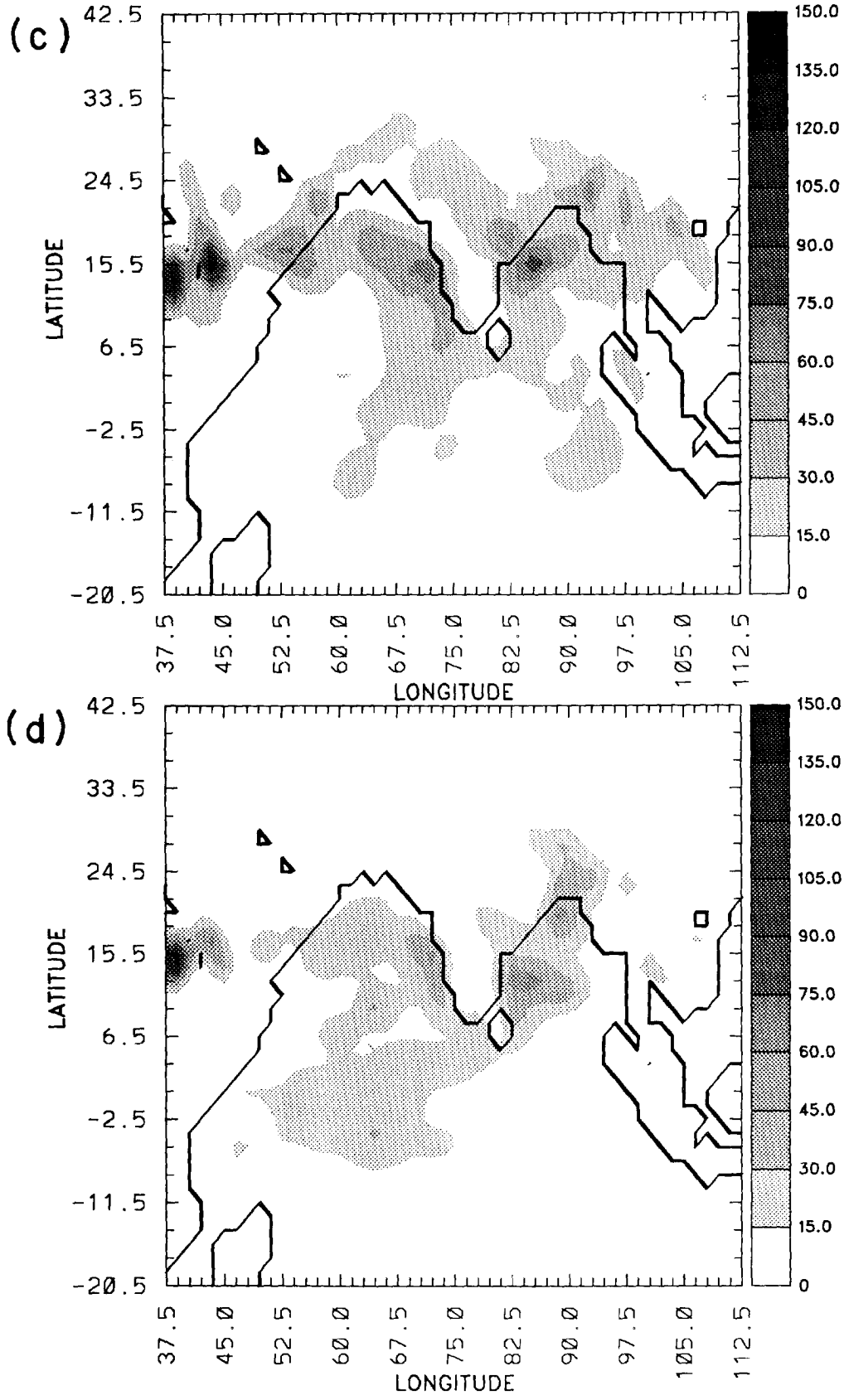

Fig. 7. Observed cumulative rainfall (mm d^{-1}) (a) ending at 03 UTC 17 July 1988 and (b) 03 UTC 18 July 1988.7.(c) The model predicted rainfall (mm d^{-1}) in the SSTC for a period of 24 h ending (c) at 12 UTC 17 July and (d) at 12 UTC 18 July 1988.

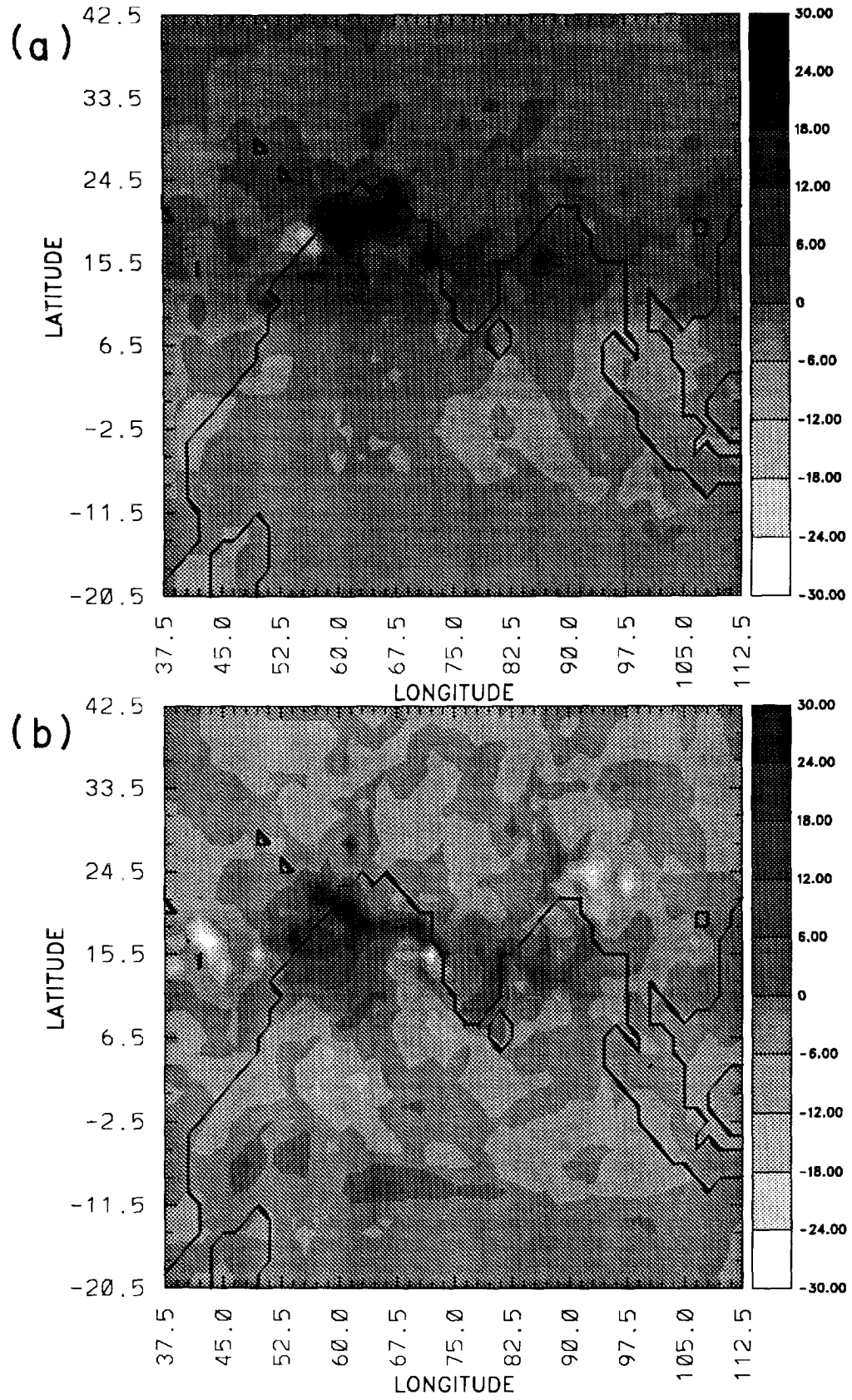

Fig. 8. Differences between the model predicted rainfall rates (mm d^{-1}) in the SSTO and the SSTC for a period of 24 h ending (a) at 12 UTC 17 July and (b) 12 UTC 18 July 1988.

available at a coarse horizontal resolution (1.875° × 1.875°), processed initial conditions for desert regions are influenced by the conditions present over the adjacent oceanic regions. As a result, model predicts rainfall over this desert region. However, predicted rainfall rates for the second day (Fig. 7d) indicated very small values over these regions. It is interesting to note that the alignment of predicted precipitation fields over the Arabian Sea in general is southwest to northeast, which is in the same direction as the

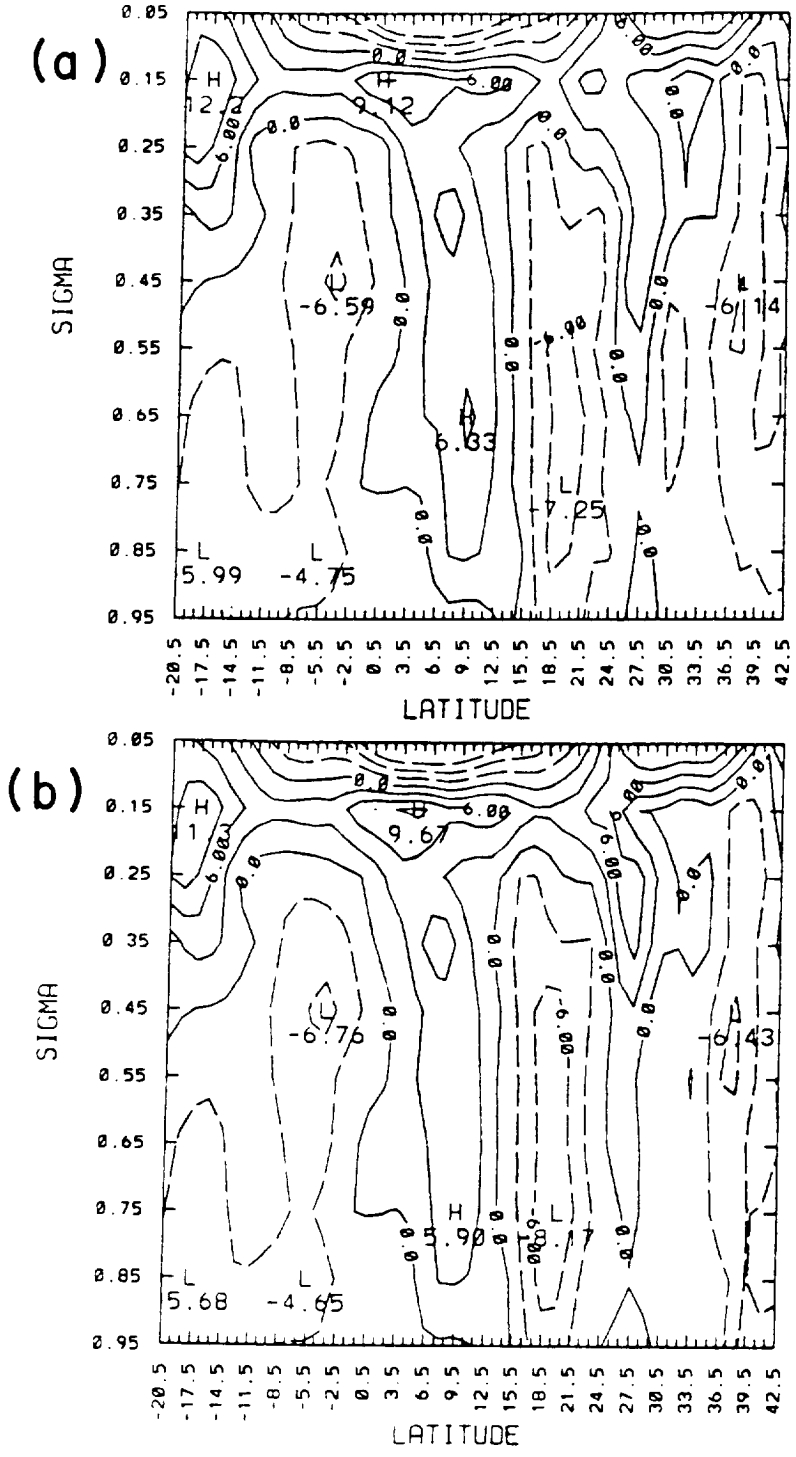

Fig. 9. Latitude-height section of the forecast errors for the zonally averaged zonal winds ($m\,s^{-1}$) at the end of 48 h of simulation (a) in the SSTO and (b) in the SSTC. Contour intervals is $3\,m\,s^{-1}$.

observed cloud bands (Bunker and Chaffee, 1969; Roadcap and Rao, 1993).

Differences between the rainfall predicted by the SSTO and the SSTC for a period of 24 h ending at 12 UTC 17 July are shown in Fig. 8a. Positive values indicate increase in the rainfall in the SSTO. During the first day of simulation the differences in the rainfall are larger over the east coast of Africa, west coast of India and the Bay of Bengal, consistent with the variations in the latent heat fluxes. There exist small regions of decreased rainfall adjacent to regions of increased rainfall. This could be due the fact that the increased rainfall is associated with the large vertical velocities and the compensating descending motions affected the surrounding circulation patterns. Differences between the rainfall predicted by the SSTO and the SSTC for a period of 24 h ending at 12 UTC 18 July are shown in Fig. 8b. In general, over the oceans a maximum of $+24$ mm d^{-1} and a minimum of about -10 mm d^{-1} in the rainfall difference is found. Also, positive anomaly in the rainfall increases over the oceans during the second day. However, increase in the rainfall rates over the land is not significant.

It will be of interest to find out which forecast is closer to the observations. For this purpose zonally averaged zonal wind fields are considered. Latitude-height section of the forecast errors (predicted minus analyzed) for the zonally averaged zonal winds in the SSTO at the end of 48 h of simulation (12 UTC 18 July) are shown in Fig. 9a and corresponding errors in the SSTC are shown in Fig. 9b. One of the distinct features present in the zonal wind field (not shown) is the presence of a low level wind maximum between 6.5° and 18.5° N, indicating the observed location of the Somali jet in the lower troposphere. Also, there exists a wind maximum at upper levels (at 0.15σ) due to the presence of the tropical easterly jet. Forecast errors in the zonal winds associated with the Somali jet and tropical easterly jet (Fig. 9a and b) are somewhat larger. Similarly, large forecast errors can also be seen over the Himalayan mountain region (30° to 42° N). This is due to coarse vertical resolution of the model and uncertainties present in the analyzed wind fields. As shown earlier (Fig. 5b), differences between the wind speeds in the SSTO and the SSTC range from 1 to 5 m s^{-1} at the lowest level of the model and hence differences in the forecast errors in zonally averaged winds in the SSTO and the SSTC are not significant. In terms of mean flow, a maximum difference of about 0.8 m s^{-1} can be seen in the errors for zonally averaged zonal winds (Fig. 9a and b). This indicates that the differences between the SSTO and the SSTC exist only in the mesoscale while the large-scale mean flow remains essentially the same.

Temporal variations of total domain average of hourly evaporation and rainfall in the SSTO and the SSTC are shown in Fig. 10. Increase of rainfall rates during the first 12 h of simulation in both the cases indicate the spinup time required by the model. Hourly rainfall in both the SSTO and the SSTC show small

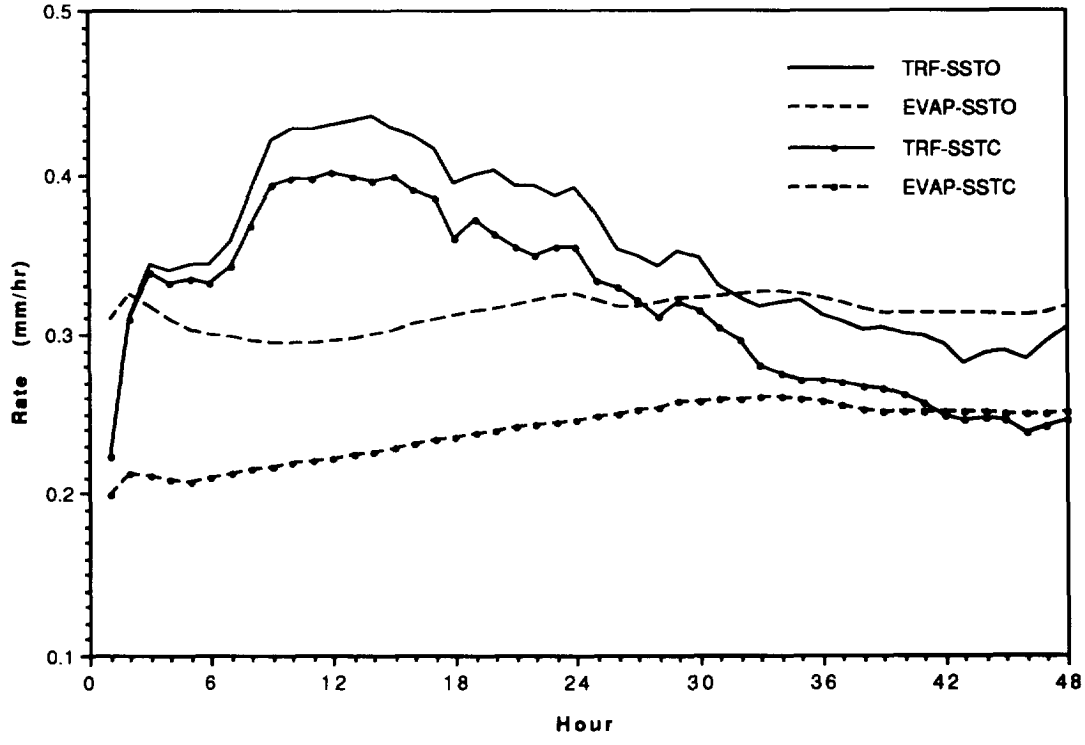

Fig. 10. Temporal variations of total domain average of hourly accumulated rainfall and accumulated evaporation rates (mm h^{-1}) in the SSTO and the SSTC.

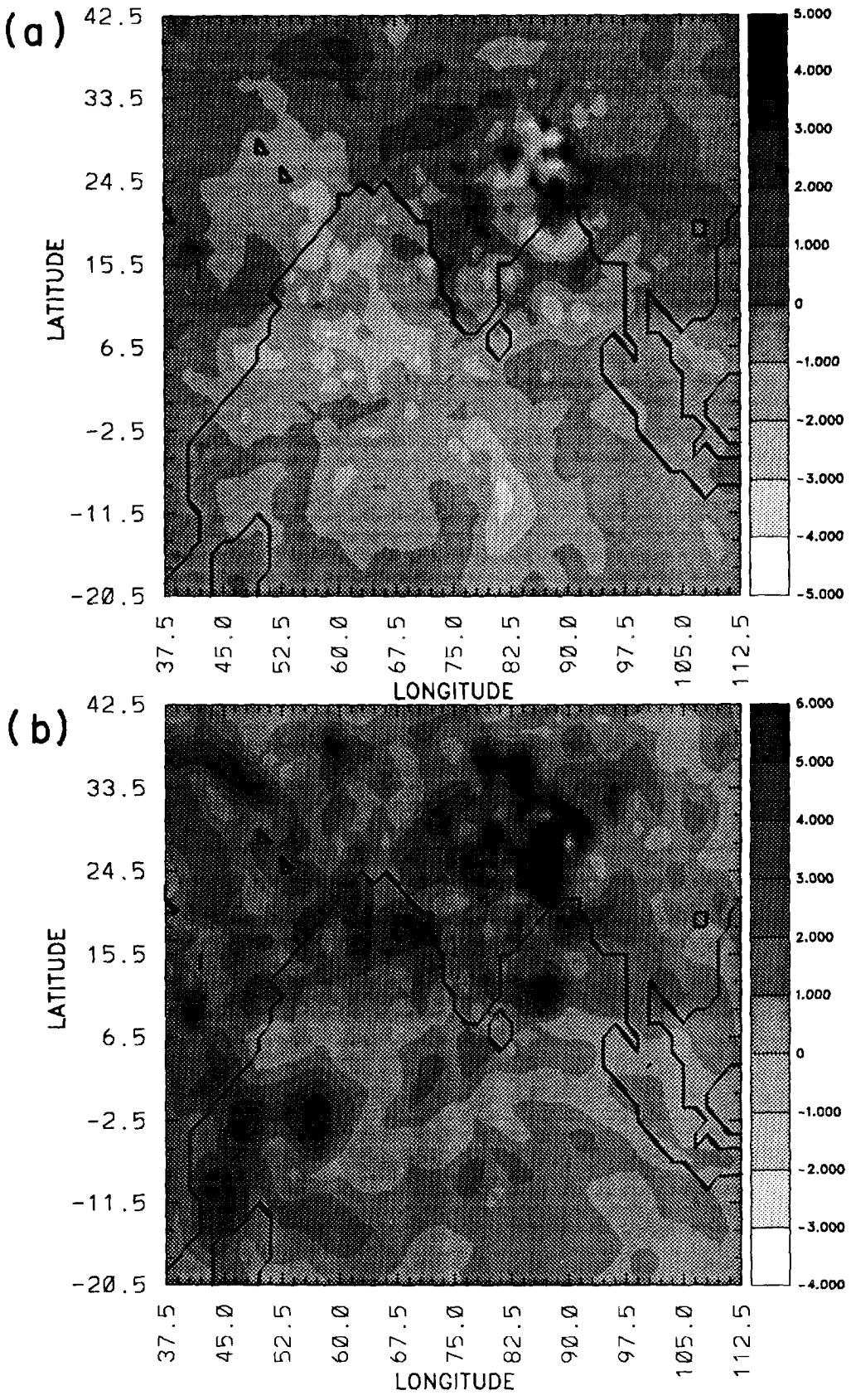

Fig. 11. Differences between the simulations in the SSTU and SSTC at the end of 48 h for (a) surface pressures (hPa) and (b) horizontal winds ($m\,s^{-1}$) at model's lowest level.

differences up to about 9 h of simulation after which they differed by about 0.05 mm h^{-1}. This difference was maintained consistently from 10 h to the end of simulation. Thus, domain-averaged rainfall in the SSTO is about 10% higher than that in the SSTC. This difference in the domain-averaged rainfall rates translates to about 0.4°C h^{-1} of heating in the area-averaged model atmosphere. As mentioned earlier, SST anomalies are present almost all over the Arabian Sea and other oceanic regions. Hence, a lag in the evaporation and rainfall rates does not exist in the SSTO. It was shown in Fig. 6 that the latent heat fluxes in the SSTO are larger than those in the SSTC. Consistently, hourly evaporation rates are also higher in the SSTO and this positive difference is maintained persistently (Fig. 10) with an average value of 0.07 mm h^{-1} while the differences in the rainfall rates are maintained at an average of 0.05 mm h^{-1}. This indicates that the low levels of the atmosphere in the SSTO is more moist than that in the SSTC. Also, as can be seen from Fig. 10 evaporation exceeds the rainfall after 31 h of simulation in the SSTO.

3.2. *Sensitivity of the model to the uniform increase in the climatological SSTs*

Since the differences between the observed SSTs and the climatological SSTs are about 1 to 2°C and are nonuniform, it will be interesting to study the effect of uniformly increased climatological SSTs by 2°C on the model predictions. For this purpose the climatological SSTs are uniformly increased by 2°C and numerical simulations are performed for 48 h starting at 12 UTC 16 July. Results from this experiment are referred to as SSTU.

Differences between the predicted surface pressures in the SSTU and the SSTC at the end of 48 h (12 UTC 18 July) of simulation are shown in Fig. 11a. Uniformly increased SSTs lead to lower surface pressures. In general, there is a larger surface pressure decrease in the SSTU as compared to that in the previous simulation. Differences between the predicted horizontal wind speeds at the lowest level of the model in the SSTU and the SSTC at the end of 48 h of simulation are shown in Fig. 11b. Since SSTs are uniformly increased, horizontal SST gradients remain same.

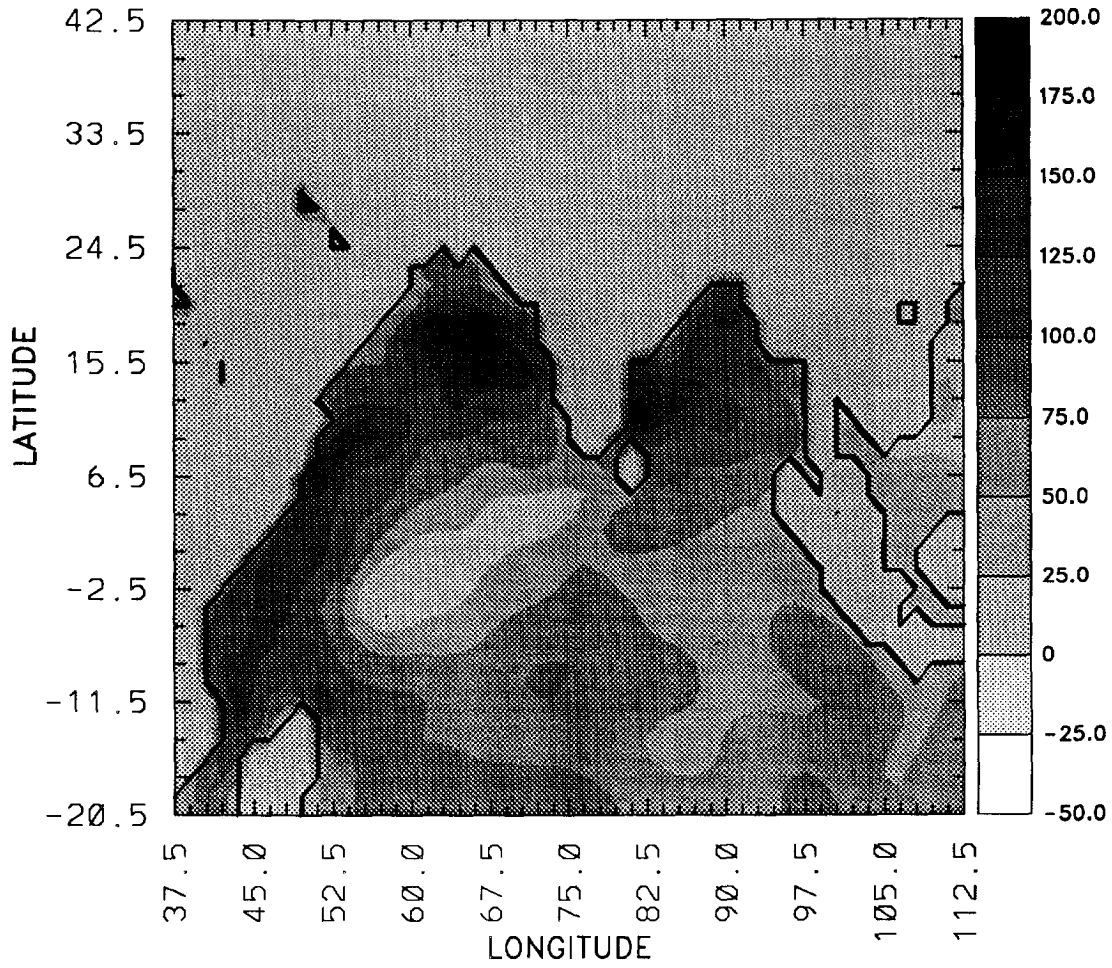

Fig. 12. Differences between predicted mean latent heat fluxes (W m^{-2}) in the SSTU and the SSTC at the end of 48 h.

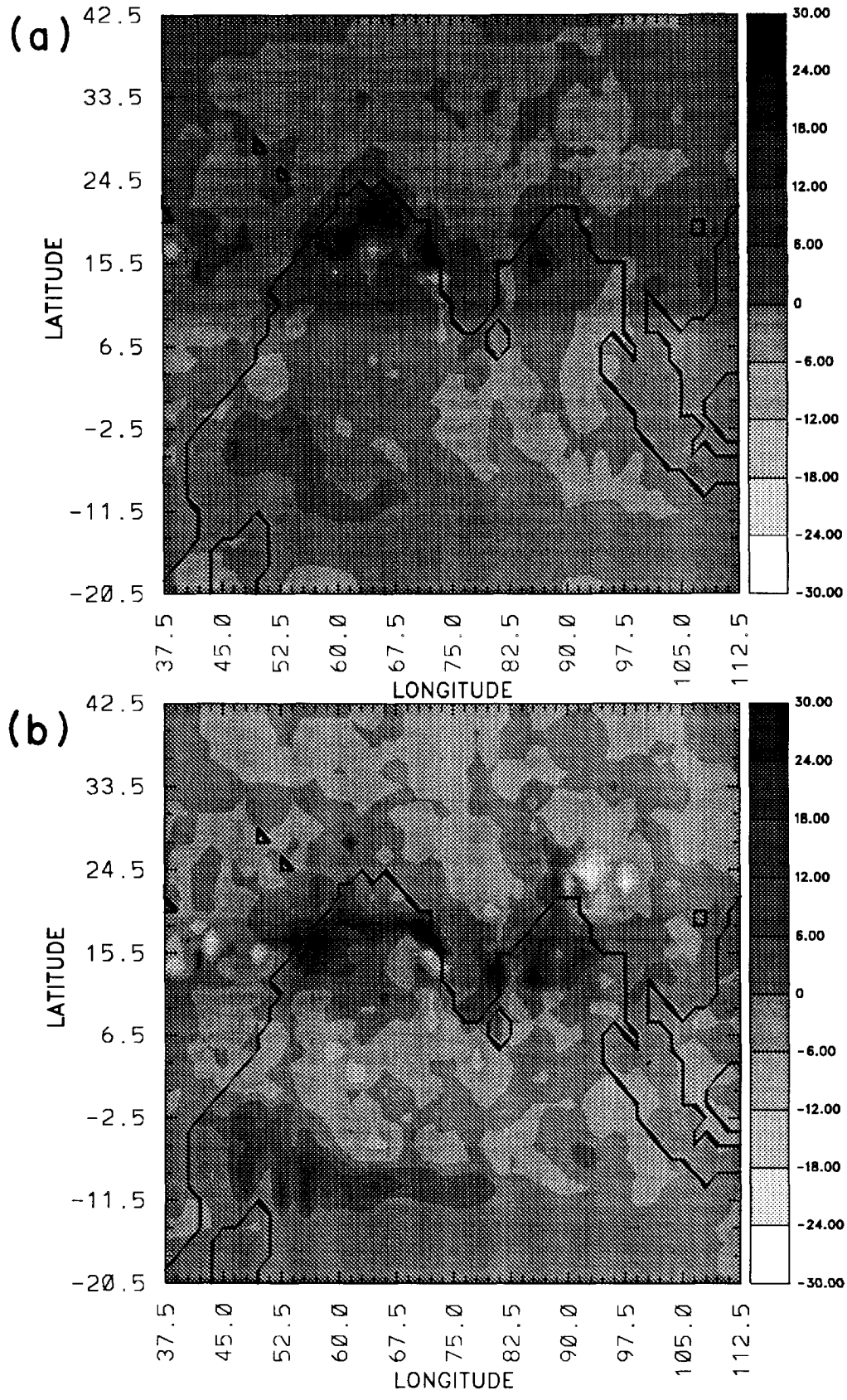

Fig. 13. Differences between the model predicted rainfall rates (mm d^{-1}) in the SSTU and the SSTC for a period of 24 h ending (a) at 12 UTC 17 July and (b) at 12 UTC 18 July 1988.

Consistently, predicted wind speeds in the SSTC and the SSTU simulations are somewhat similar during the first day of simulation. However, predicted wind speeds varied during the second day (Fig. 11b), possibly due to the significant differences in the magnitudes of the mesoscale circulations in the SSTC and the SSTU. Also, differences in the predicted latent heat fluxes between the SSTU and SSTC are also higher during the second day of simulation (Fig. 12). Maximum increase in the latent heat fluxes in the SSTU is about 150 W m^{-2} located near the east coast of Africa and also near the east coast of India.

Differences between the rainfall rates predicted by the SSTU and the SSTC for a period of 24 h ending at 12 UTC 17 July are shown in Fig. 13a. There is an increase in the rainfall for the SSTU along the west coast of India and over the location of the monsoon depression. Differences in the predicted rainfall rates for the second day of simulation between the SSTU and the SSTC are shown in Fig. 13b. Compared to the previous day, the difference in the rainfall is even larger over the oceans. Uniform increase in the SSTs by 2°C in the SSTU caused near-surface air to be more humid than those present in the SSTC, resulting in increased evaporation. As discussed earlier, a uniform increase in the SSTs does not change the horizontal gradients, but caused increased evaporation and decreased surface pressure. This causes increase in convection which in turn influences the dynamics of the flow through baroclinic effects. Consistently, computed vertical velocities (not shown) also indicate higher values over the regions of intense cumulus convection.

In all the simulations (SSTO, SSTC and SSTU), predicted locations of the monsoon depression at the end of 48 h of simulation are very similar. Also, the differences in the predicted rainfall rates associated with the monsoon depression between SSTO and SSTC and also between SSTU and SSTC are positive. These results suggest that an increase in the SSTs can cause increased rainfall rates (as much as 20 mm d^{-1}) associated with the monsoon depression while its track and intensity (as indicated by the surface pressure) are very similar.

Temporal variations of total domain average of hourly evaporation and rainfall rates in the SSTO, SSTC and the SSTU are shown in Fig. 14. Hourly rainfall rates in the SSTO and the SSTU are very similar up to about 9 h of simulation after which they differed on average by about 0.03 mm h^{-1} up to 30 h. After this, the differences reduced to about 0.02 mm h^{-1}. Evaporation exceeds the rainfall after 41 h in the SSTC, after 31 h in the SSTO and after 29 h in the SSTU as result of warmer SSTs. Also, evaporation exceeds the rainfall by a larger amount in the SSTU than that in the SSTC and SSTO. In general, when domain averages are considered, uniform increase of SSTs by 2°C leads to an increase of evaporation by about 40% and rainfall by about 15%.

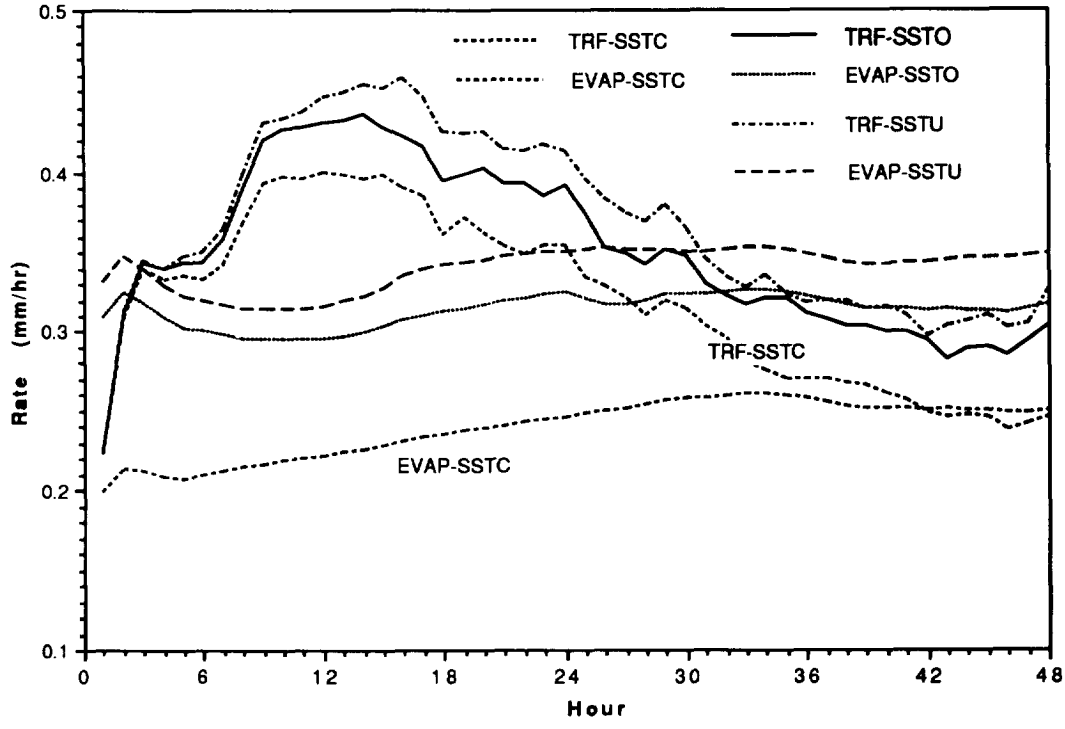

Fig. 14. Temporal variations of total domain average of hourly accumulated rainfall and accumulated evaporation rates (mm h^{-1}) in the SSTC, SSTO and SSTU.

4. CONCLUSIONS

Sensitivity of the summer monsoon rainfall to the changes in the sea surface temperatures (SSTs) was studied in the context of short-range weather forecast. Results indicate that the changes in the SSTs affect the dynamics and the thermodynamics of the monsoon flow in a very consistent manner. Observed SSTs are found to be about 1 to 2°C warmer than the climatological values locally. As a result, lower surface pressures and stronger winds are predicted because of the gradients in the observed SSTs. Further, these changes led to the prediction of increased evaporation by about 20% and rainfall by about 10% when domain averages are considered. A uniform increase by 2°C in the climatological SSTs led to increased evaporation, resulting in increased spatial distribution and higher rainfall rates. In turn, increased rainfall lead to stronger circulation patterns. Increased evaporation over the oceans appears to be mainly due to the increase in the SST. There was a 40% increase in the area-averaged evaporation and a 15% increase in rainfall rates when a uniform warming (2°C) of the sea surface was considered.

These differences in the model predictions suggest that the sea surface temperature is a crucial parameter in the prediction of monsoon rainfall. In the context of the short-range weather prediction, differences do exist in the mesoscale circulations and associated physical processes while the large-scale mean flow in general is marginally different for small variations in the SSTs.

Acknowledgements—This work was supported in part by the Naval Research Laboratory and by the Division of International Programs, National Science Foundation by Grant INT-9008926. Computer resources were provided by the North Carolina Supercomputing Center, Research Triangle Park, NC.

REFERENCES

Anjaneyulu T. S. S. (1980) A study of air and sea surface temperatures over the Indian Ocean. *Mausam.* **31,** 551–560.

Anthes R. A. (1977) Hurricane model experiments with a new cumulus parameterization scheme. *Mon. Wea. Rev.* **105,** 287–300.

Bourke W. and McGregor J. L. (1983) A nonlinear vertical mode initialization scheme for a limited area prediction model. *Mon. Wea. Rev.* **111,** 2285–2297.

Briere S. (1982) Nonlinear normal mode initialization of a limited area model. *Mon. Wea. Rev.* **110,** 1166–1186.

Bunker A. F. and Chaffee M. (1969) *Tropical Indian Ocean Clouds.* East-West Center Press, University of Hawaii, 193.

Businger J. A., Wyngaard J. C. Izumi Y. and Bradley E. F. (1971) Flux-profile relationship in the atmospheric surface layer. *J. Atmos. Sci.* **28,** 181–189.

Cadet D. and Reverdin G. (1981) Water vapour transport over the Indian Ocean during summer 1975. *Tellus* **33,** 476–487.

Das S., Mohanty U. C. and Sharma O. P. (1988) Study of Kuo-type cumulus parameterizations during different epochs of the Asian summer monsoon. *Mon. Wea. Rev.* **116,** 715–729.

Davies H. C. (1976) A lateral boundary formulation for multi-level prediction models. *Quart. J. Roy. Meteor. Soc.* **102,** 405–418.

Davies H. C. (1983) Limitations of some common lateral boundary schemes used in regional NWP models. *Mon. Wea. Rev.* **111,** 1002–1012.

Holt T. and Sethu Raman S. (1985) Aircraft and ship observations of the mean structure of the marine boundary layer over the Arabian sea during MONEX 79. *Boundary-Layer Meteorol.* **33,** 259–282.

Joseph P. V. and Pillai P. V. (1984) Air–sea interaction on seasonal scale over north Indian Ocean. Part 1: Interannual variations of sea surface temperature and Indian summer monsoon rainfall. *Mausam.* **35,** 323–330.

Krishnamurti T. N. and Bhalme H. N. (1977) Oscillations of a monsoon system. Part I. Observational aspects. *J. Atmos. Sci.* **33,** 1937–1954.

Krishnamurti T. N., Cocke, S., Pasch R. and Low-Nam S. (1983) Precipitation estimates from rainguage and satellite observations: Summer MONEX. Dept. of Meteorology, Florida State University.

Kuo H. L. (1965) On the intensification of tropical cyclones through latent heat release by cumulus convection. *J. Atmos. Sci.* **22,** 40–63.

Kuo H. L. (1974) Further studies of the parameterization of the influence of cumulus convection on large-scale flow. *J. Atmos. Sci.* **31,** 1232–1240.

Kusuma G. R. and Goswami B. N. (1988) Inter-annual variation of sea surface temperature over the Arabian Sea and the Indian monsoon: A new perspective. *Mon. Wea. Rev.* **116,** 558–568.

Madala R. V., Chang, S. W., Mohanty U. C., Madan S. C., Paliwal R. K., Sarin V. B., Holt T. and Raman S. (1987) Description of the Naval Research Laboratory limited area dynamical weather prediction model. NRL Memo. Rep., No. 5992, Naval Research Laboratory, Washington, D.C.

Ramachandran G. (1972) The role of orography on wind and rainfall distribution in and around a mountain gap: Observational study. *Indian J. Meteor. Geophys.* **23,** 41–44.

Ramage C. S. (1971) *Monsoon Meterology,* pp. 37–194. Academic Press, New York.

Ramakrishnan K. P. and B. Gopinatha Rao (1958) Some aspects of the nondepressional rain in peninsular India during the southwest monsoon. *Pro. Symp. on the Monsoon World,* Indian Meteorological Department.

Ramesh Babu V., Subba Rao M. and Rao M. V. (1989) Influence of eastern Arabian Sea on summer monsoon rainfall over west coast of India. *Vayu Mandal,* July–December, 75–78.

Rao Y. P. (1976) Southwest Monsoon. Meteorological Monograph, Synoptic Meteorology No. 1/1976, India Meteorological Department, India., pp 367.

Roadcap J. R. and Rao G. V. (1993) An analytical study of the dependence of orientation and propagation of the Arabian Sea convection bands on wind shear, static stability, and preexisting convection. *Mon. Wea. Rev.* **121,** 1656–1670.

Saha K. R. and Bavadekar S. N. (1973) Water vapour budget and precipitation over the Arabian Sea during the Northern Summer. *Quar. J. Roy. Meteorol. Soc.* **99,** 272–278.

Sashegyi K. D. and Madala R. V. (1990) Test of initialization procedures with the NRL limited area numerical weather prediction model. NRL Memo. Rep., No. 6648, Naval Research Laboratory, Washington, D. C.

Shukla J, (1975) Effect of Arabian Sea surface temperature anomaly on Indian summer monsoon: A numerical experiment with GFDL model. *J. Atmos. Sci.* **32,** 503–511.

Simon B. and Desai P. S. (1991) Estimation of heat fluxes over Indian Ocean using satellite Data. In Proc.Indo–US Seminar on Parameterization of Sub-grid Scale Processes in Dynamical Models of Medium Range Prediction and Global Climate, pp. 193–199. IITM, Pune, India.

Van de Boogaard H. and Rao G. V. (1984) Mesoscale

structures of the low-level flow near the equatorial East African Coast. *Mon. Wea. Rev.* **112,** 91–107.

Washington W. M., Chervin R. V. and Rao G. V. (1977) Effects of a variety of Indian Ocean surface temperature anomaly patterns on summer monsoon circulation: Experiments with NCAR GCM. *Pure. Applied Geophysics.* **115,** 1335–1355.

Weare B. C. (1976) Statistical study of the relationship between ocean surface temperatures and Indian monsoon. *J. Atmos. Sci.* **36,** 2279–2291.